



**HAL**  
open science

## Photolysis of multifunctional carbonyl compounds under natural irradiation at EUPHORE

Alexandre Tomas, L. Aslan, A. Muñoz, M. Ródenas, T. Vera, E. Borrás, P. Coddeville, C. Fittschen

► **To cite this version:**

Alexandre Tomas, L. Aslan, A. Muñoz, M. Ródenas, T. Vera, et al.. Photolysis of multifunctional carbonyl compounds under natural irradiation at EUPHORE. *Atmospheric Environment*, 2021, 253, pp.118352. 10.1016/j.atmosenv.2021.118352 . hal-04221749

**HAL Id: hal-04221749**

**<https://hal.science/hal-04221749v1>**

Submitted on 20 Oct 2023

**HAL** is a multi-disciplinary open access archive for the deposit and dissemination of scientific research documents, whether they are published or not. The documents may come from teaching and research institutions in France or abroad, or from public or private research centers.

L'archive ouverte pluridisciplinaire **HAL**, est destinée au dépôt et à la diffusion de documents scientifiques de niveau recherche, publiés ou non, émanant des établissements d'enseignement et de recherche français ou étrangers, des laboratoires publics ou privés.

1 **Photolysis of multifunctional carbonyl compounds under natural irradiation at**  
2 **EUPHORE**

3  
4  
5 **A. Tomas<sup>1,\*</sup>, L. Aslan<sup>1</sup>, A. Muñoz<sup>2,\*</sup>, M. Ródenas<sup>2</sup>, T. Vera<sup>2</sup>, E. Borrás<sup>2</sup>, P.**  
6 **Coddeville<sup>1</sup>, C. Fittschen<sup>3</sup>**

7  
8  
9  
10 <sup>1</sup> IMT Lille Douai, Institut Mines-Télécom, Univ. Lille, Center for Energy and Environment, F-59000  
11 Lille, France

12  
13 <sup>2</sup> Fundación CEAM - EUPHORE Laboratories, C/Charles R. Darwin 14, Parque Tecnológico, 46980  
14 Paterna - Valencia, Spain

15  
16 <sup>3</sup> Université Lille, CNRS, UMR 8522 - PhysicoChimie des Processus de Combustion et de  
17 l'Atmosphère (PC2A) 59000 Lille, France

18  
19  
20 \* Corresponding authors:

21 Alexandre TOMAS, Tel.: 33 327 712 651, [alexandre.tomas@imt-lille-douai.fr](mailto:alexandre.tomas@imt-lille-douai.fr)

22 Amalia MUÑOZ, [amalia@ceam.es](mailto:amalia@ceam.es)

23  
24  
25  
26 Manuscript prepared for submission to Atmospheric Environment

27

28

29 **Abstract**

30  
31 Photolysis is one the main drivers in atmospheric chemistry. Volatile organic  
32 compounds that bear one or more carbonyl functions can absorb UV light between  
33 295 nm and 450 nm, enabling them to possibly photolyze in the atmosphere. Yet,  
34 very few data are available regarding the impact of such photolysis processes on the  
35 fate of multifunctional carbonyls. In the present work, we investigated the  
36 photodissociation of one  $\alpha$ -diketone and three hydroxyketones under real sunlight at  
37 the European Photoreactor EUPHORE. The obtained photolysis frequencies  
38 normalized by  $\text{NO}_2$  photolysis were: 2,3-pentanedione (PTD):  $(3.4 \pm 0.6) \times 10^{-2}$ , 4-  
39 hydroxy-4-methyl-2-pentanone (4H4M2P):  $(6.2 \pm 2.9) \times 10^{-4}$ , 3-hydroxy-3-methyl-2-  
40 butanone (3H3M2B):  $(8.2 \pm 4.9) \times 10^{-4}$ , and 4-hydroxy-3-hexanone (4H3H):  
41  $(5.1 \pm 3.0) \times 10^{-4}$ . These ratios represent the first data for three of them, to our  
42 knowledge. Reaction products were also investigated and carbon balances of 70-  
43 100% in the gas-phase have been obtained. A photolysis reaction mechanism is  
44 proposed for 4H3H for the first time, based on the observed products. Atmospheric  
45 lifetimes span between 39 min for PTD to 1-2 days for hydroxyketones. The present  
46 work shows that photolysis of multi-oxygenated VOCs may be significant and needs  
47 to be taken into account in atmospheric chemistry models where it represents an  
48 additional source of radicals.

49  
50  
51  
52  
53  
54  
55  
56  
57  
58

59 **Keywords:** Oxygenated-VOCs; lifetime; atmosphere; dione; hydroxyketones;  
60 photolysis

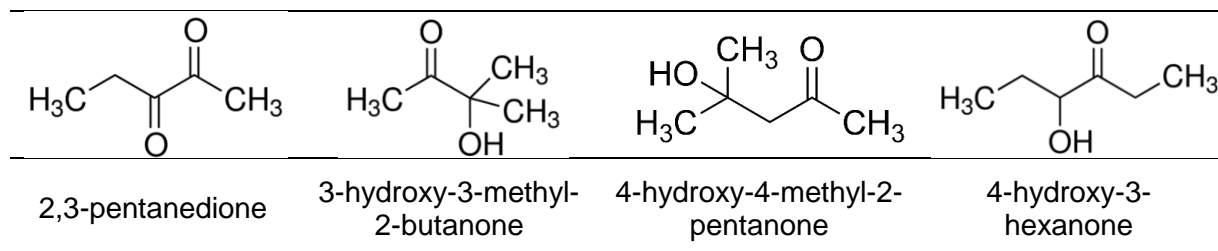
61

## 62 1. Introduction

63  
64 Photolysis of carbonyls is known to be a significant source of radicals in the  
65 atmosphere, impacting the budget of HO<sub>x</sub> and NO<sub>x</sub> on regional to global scales. Yet,  
66 measurements of photolysis frequencies under natural sunlight are rather scarce and  
67 often concern simple species like formaldehyde, acetaldehyde and acetone (Calvert  
68 et al., 2011). For most of the carbonyls, in the absence of direct measurements,  
69 photolysis frequencies can be estimated from solar actinic flux and absorption cross  
70 sections assuming quantum yields of unity, but this leads to upper limit values and  
71 (often) to an overestimation of photolysis rates (Moortgat, 2001). Indoor simulation  
72 chambers with actinic lamps may be used more easily, but high uncertainties in the  
73 photolysis frequencies may result due to the different irradiation spectrum. Accurate  
74 photolysis frequencies are one of the main uncertainties in atmospheric chemistry  
75 models like MCM or GECKO-A (Hodzic et al., 2015), especially for larger and  
76 multifunctional carbonyl compounds. Measurements under real sunlight are thus  
77 clearly necessary to gain knowledge of these radical-generating processes and to  
78 improve the consistency and robustness of atmospheric chemistry models.

79 Multifunctional carbonyl compounds like diketones and hydroxyketones represent  
80 important groups of oxygenated Volatile Organic Compounds (VOCs) in the  
81 atmosphere. The OH radical initiated oxidation is generally considered as the main  
82 degradation pathway of oxygenated VOCs while the reaction with Cl atoms (often  
83 having a much larger rate constant (Aslan et al., 2017a; Bouzidi et al., 2017)) may be  
84 significant in coastal areas where Cl atom concentrations are high. A range of recent  
85 studies has indicated that the atmospheric photolysis of multifunctional carbonyls  
86 could be significant (Aslan et al., 2017c; Bouzidi et al., 2014b, a, 2015b, a;  
87 Messaadia et al., 2012, 2015). The compounds investigated in these studies were  
88 dicarbonyls and hydroxycarbonyls that may either be directly emitted into the  
89 atmosphere or be produced in the degradation of hydrocarbons and oxygenated  
90 compounds, as suggested by laboratory studies (Grosjean and Grosjean, 1998;  
91 Reisen et al., 2003; Tuazon et al., 1998) and detailed atmospheric chemistry models  
92 (Aumont et al., 2005). In the aforementioned studies, the atmospheric photolysis  
93 rates were either calculated based on solar actinic flux and absorption cross sections  
94 or measured using indoor simulation chambers with actinic lamps. Thus, significant  
95 uncertainties remain on the importance of the photolysis channel for these species  
96 and on reaction chemical mechanisms. Photolysis rate measurements under natural  
97 sunlight are required in order to assess correctly the atmospheric significance of the  
98 photolysis pathway for these compounds.

99 The present work focused on an  $\alpha$ -dicarbonyl (2,3-pentanedione/PTD) and three  
100 hydroxycarbonyl compounds (3-hydroxy-3-methyl-2-butanone/3H3M2B, 4-hydroxy-4-  
101 methyl-2-pentanone/4H4M2P and 4-hydroxy-3-hexanone/4H3H) aiming at measuring  
102 their photolysis rates under natural irradiation and comparing with artificial light  
103 studies.  
104



105

106 These compounds were chosen to identify possible structure-activity relationships  
107 regarding their photodissociation rates. The studies were carried out at the outdoor  
108 European Photoreactor (EUPHORE). This facility allows the experiments to be  
109 performed under realistic atmospheric conditions, particularly with respect to the  
110 intensity and wavelengths of solar radiation. The main primary products of the  
111 photolysis of PTD, 3H3M2B, 4H4M2P and 4H3H were determined. The results are  
112 discussed in terms of the impact of the direct photolysis of multifunctional carbonyls  
113 as a source of radicals and carbonyls in the atmosphere.

114

## 115 **2. Experimental section**

116

117 The EUPHORE chamber is a hemispheric Teflon reactor of  $\sim 200 \text{ m}^3$  that can be  
118 exposed to sunlight when uncovered. A thorough description can be found in  
119 (Becker, 1996; Muñoz et al., 2011). The experiments took place between 12<sup>th</sup> and  
120 21<sup>st</sup> of July 2017 with overall sunny days though the sky was sometimes partly  
121 covered by clouds. Averaged  $\text{NO}_2$  photolysis rates (determined by  
122 spectroradiometry) laid in the range  $0.45$  to  $0.56 \text{ min}^{-1}$  (see Table 1).

123 Two experiments were carried out for each selected compound: one with an OH-  
124 radical scavenger (cyclohexane) where more than 93% of OH reacted with the  
125 scavenger (see Table 1), the other one in the absence of scavenger. Reactants and  
126 products were measured using five different techniques: 1) in situ Fourier Transform  
127 Infrared (FTIR) spectroscopy with an optical pathlength of 554 m; 2) Proton-Transfer  
128 Reaction Mass Spectrometry (PTR-MS); 3) Gas Chromatography (GC) with Photo  
129 Ionization Detection (PID) and Flame Ionization Detection (FID); 4) Gas  
130 Chromatography Mass Spectrometry (GC-MS) with auto SPME (solid phase  
131 microextraction) sampling and 5) Liquid Chromatography with Mass Spectrometry  
132 (LC-MS). A UV absorption based  $\text{O}_3$  monitor (Ecotech Serinus10) was also used as  
133 well as HPLC with fluorescence detection for peroxide determination. A  $\text{NO}_x$  monitor  
134 (Teledyne T200) was used to measure  $\text{NO}$ ,  $\text{NO}_2$  and  $\text{NO}_x$ . Description of the  
135 techniques and calibration methods used at EUPHORE are described elsewhere  
136 (Borrás et al., 2017; Muñoz et al., 2018; Thalman et al., 2015) and only a brief  
137 description of the conditions used for the experiments are given here. For GC and  
138 PTR-MS analysis, gas samples were taken automatically from the chamber through a  
139 slightly heated line ( $65^\circ\text{C}$  in the case of GC-MS and  $80^\circ\text{C}$  for PTR-MS). PTR-MS  
140 samples were taken automatically, in full scan mode from  $m/z$  21 to 150, with a dwell  
141 time of 1 s and E/N of 130 Td. PTR-MS quantification was made using external gas  
142 bottle calibrations (for HCHO, acetone and acetaldehyde), chamber introduction (for  
143 reactants) and software based theoretical calculations for the other products  
144 determined. IR spectra were obtained from the co-addition of 300 scans with a  
145 resolution of  $1 \text{ cm}^{-1}$ , resulting in a time resolution of about 5 min. The IR intervals  
146 used for the analysis were: PTD ( $2600\text{-}2869 \text{ cm}^{-1}$ ); 3H3M2B ( $830\text{-}1242 \text{ cm}^{-1}$ );  
147 4H4M2P ( $2650\text{-}2835.5 \text{ cm}^{-1}$ ); 4H3H ( $2650\text{-}2785 \text{ cm}^{-1}$ ); for cyclohexane, the analysis  
148 region was around  $2700 \text{ cm}^{-1}$  and varied depending on the oxygenated reactant.

149 The determination of hydroperoxides and organic peroxides by HPLC has been  
150 optimized at EUPHORE based on the reaction of  $\text{H}_2\text{O}_2$  and organic  
151 hydroperoxides/peroxides with p-hydroxyphylacetic acid to form a fluorescent dimer  
152 using peroxidase as an enzyme catalyst (Morgan and Jackson, 2002). An Agilent  
153 HPLC system (Santa Clara, USA) with a 1100 thermostated autosampler, column  
154 compartment and fluorescence detector with a 1260 binary pump was used. Water at

155 pH=3.5 was used as mobile phase at 0.5 mL/min, column used (Purospher RP-18e-,  
156 250x4 mm, 5 um from Merck) was thermosthatized at 5°C and 100 uL of sample was  
157 the injection volume.

158 GC-MS analysis was preceded by sampling on a Solid-Phase Micro-Extraction  
159 (SPME) needle with PFBHA as derivatization agent (Thalman et al., 2015). A  
160 sampling cell was designed for adapting the input from a high-volume simulation  
161 chamber. The air passed through, in a turbulent regime at 10 L min<sup>-1</sup> during a  
162 selected sampling time. The sample is thermally desorbed in the GC port of an  
163 Agilent GC-MS (Santa Clara, USA) equipped with a HP-5MS column of 30 m × 0.25  
164 mm I.D × 0.25 mm film. The chromatograph was programmed at 80°C for 2 min, then  
165 ramped at a rate of 12°C min<sup>-1</sup> to 240°C, 100°C min<sup>-1</sup> to 280°C. The injection port was  
166 held at 250°C and the transfer line from GC to MS was held at 300°C. Samples were  
167 injected in splitless mode, using helium as carrier at a flow of 1 mL min<sup>-1</sup>. The EI-  
168 voltage was 70 eV, the ion source temperature at 200°C and the quadrupole  
169 temperature at 100°C. Full scan mode was used (m/z 50-650) to identify the most  
170 abundant ions of carbonyl derivatives. The selected ion chromatograms of the most  
171 abundant ions were used to quantify the concentration of derivatives in solution.

172 The procedure for a typical experiment was as follows: liquid samples of reactants  
173 were introduced into the chamber by a stream of heated air with the fans switched on  
174 to assure a homogeneous mixture of the air mass, and stood in the dark for about 30  
175 min allowing the loss rates (wall losses and dilution) to be evaluated. The dilution rate  
176 was checked following the SF<sub>6</sub> (inert compound injected after the reactants) evolution  
177 by FTIR. The chamber was then opened and exposed to sunlight for about 5h. Initial  
178 reactant concentrations and irradiation conditions are summarized in Table 1.

179 Reactants were obtained from commercial sources. PTD (> 97%), 3H3M2B (> 95%),  
180 4H4M2P (> 99%), 4H3H (not specified but probably > 95% from our own GC  
181 analysis) and cyclohexane (> 99.9%) were all from Sigma-Aldrich. SF<sub>6</sub> (99.9%) was  
182 from Abelló Linde. All compounds were used as received without further purification.

183

### 184 3. Results and Discussion

185

#### 186 3.1 Photolysis frequencies

187 Photolysis being a first-order process, the rate coefficients (also called photolysis  
188 frequencies) can be determined from the time-dependent reactant concentrations *C*  
189 using:

190

$$191 \ln\left(\frac{C_0}{C}\right) = J_{VOC,obs} \times t \quad (\text{Eq. 1})$$

192

193 where  $J_{VOC,obs}$  is the observed decay rate, the subscript *0* denoting the initial reactant  
194 concentration and *t* being the reaction time. Eq. 1 shows that only relative  
195 concentrations are needed to retrieve  $J_{VOC,obs}$ . For hydroxyketones, FTIR data were  
196 used to determine the photolysis frequencies; the other data from PTR-MS and GC  
197 analysis, while providing consistent results with FTIR (generally within 30%),  
198 presented higher uncertainties, mainly because of a much lower number of data (GC  
199 measurements with low time resolution) and more data scattering (PTR-MS using a  
200 quadrupole mass filter). For PTD, data from FTIR, GC and PTR-MS were used.

201 The corresponding kinetic plots are given in Figures 1a to 1d for 4H4M2P, PTD,  
202 3H3M2B and 4H3H, respectively. The observed decay rates were then corrected for  
203 dilution and wall losses using the FTIR data recorded before opening the chamber.

204 The corrected photolysis frequency for each compound ( $J_{VOC,corr}$ ) averaged over the

205 entire exposure time was determined using the experiments carried out with OH  
206 scavenger. A similar data analysis was done for the experiments carried out without  
207 OH scavenger (Figures S1a to S1d). The corrected first order rates obtained in these  
208 later experimental conditions correspond to both photolysis and OH reaction. Finally,  
209 an average NO<sub>2</sub> photolysis frequency ( $J_{NO_2}$ ) was calculated from the  
210 spectroradiometer data over the whole irradiation period.  $J_{NO_2}$  values range from  
211  $0.45 \pm 0.10 \text{ min}^{-1}$  to  $0.56 \pm 0.07 \text{ min}^{-1}$ , the error ( $1\sigma$ ) representing the fluctuation of  
212 irradiance during photolysis time (Table 1).

213 The results are summarized in Table 2. The observed  $J_{VOC,obs}$  are around  $1 \times 10^{-3} \text{ min}^{-1}$   
214 for hydroxyketones and  $2 \times 10^{-2} \text{ min}^{-1}$  for PTD. After wall loss and dilution  
215 corrections, the hydroxyketone photolysis frequencies fall around a few  $10^{-4} \text{ min}^{-1}$   
216 and represent only a fraction of the observed decay rates (~20-30%), the main part  
217 being wall loss and dilution. Conversely, for PTD, the correction represents only  
218 about 5%. Uncertainties on  $J_{VOC,corr}$  arise from errors on  $C_0/C$  (about 2% statistical)  
219 and on the wall loss and dilution rates (about 15%). Propagating the errors yields  
220 global errors between 2% (for PTD) up to 45% (for 4H3H) on  $J_{VOC,corr}$ .  $J_{VOC,corr}$  were  
221 then normalized by  $J_{NO_2}$ . It is worth noting that the difference in the  $J_{VOC,corr}/J_{NO_2}$   
222 ratios with and without OH scavenger is rather low for hydroxyketones (of the order of  
223 20-40% which is within the uncertainties) and even negligible for PTD. Yet, in all  
224 experiments carried out with cyclohexane, cyclohexanol and cyclohexanone  
225 (products of cyclohexane + OH) were observed by GC-MS, suggesting that OH  
226 radicals are still formed in all chemical systems. OH radicals may be formed in  
227 peroxy radical reactions (Orlando and Tyndall, 2012).  
228

229 Table 2 also reports literature data on photolysis frequencies of the investigated  
230 compounds. To the best of our knowledge, only one study is available regarding  
231 photolysis frequency measurements performed under natural irradiation (Magneron  
232 et al., 2003). This determination was performed at EUPHORE and concerned  
233 4H4M2P. The present determination of  $J_{4H4M2P,corr} = (3.4 \pm 1.1) \times 10^{-4} \text{ min}^{-1}$   
234 ( $J_{VOC,corr}/J_{NO_2} = (6.2 \pm 2.9) \times 10^{-4}$ ) is consistent with their upper limit of  $3.0 \times 10^{-4} \text{ min}^{-1}$   
235 ( $J_{VOC,corr}/J_{NO_2} < 5.4 \times 10^{-4}$ ). The inability of Magneron et al. to determine the photolysis  
236 frequency may be due to a higher dilution rate at the time of their experiments. Other  
237 investigations in the literature were carried out using actinic lamps emitting near 310  
238 nm (Aslan et al., 2017c, b; Bouzidi et al., 2014b) or 360 nm (Bouzidi et al., 2014a).  
239 The present results are in reasonable agreement with photolysis frequencies from  
240 literature and can be considered as satisfactory taking into account that different  
241 irradiation systems were used.

242 Photolysis rates can also be calculated using the actinic flux measured at EUPHORE  
243 and the known absorption cross sections  $\sigma_{VOC}(\lambda)$  of the targeted compounds (Aslan  
244 et al., 2017b, c; Messaadia et al., 2012; Szabo et al., 2011) using the following  
245 formula:

$$247 \quad J_{calc,VOC} = \int \sigma_{VOC}(\lambda) \times \Phi_{VOC}(\lambda) \times F(\lambda) d\lambda \quad (\text{Eq. 2})$$

248  
249 where  $\Phi_{VOC}(\lambda)$  is the wavelength-dependent quantum yield assumed to be equal to  
250 unity at all  $\lambda$  and  $F(\lambda)$  is the actinic flux at EUPHORE.  $F(\lambda)$  was determined by  
251 adjusting the actinic flux at 40°N, 1<sup>st</sup> July (Demerjian et al., 1980) to the averaged  
252  $J_{NO_2}$  measured values. The calculated photolysis rates,  $J_{calc,VOC}$  for 4H4M2P, PTD,  
253 3H3M2B and 4H3H were found to be  $1.5 \times 10^{-3} \text{ min}^{-1}$ ,  $7.9 \times 10^{-2} \text{ min}^{-1}$ ,  $1.4 \times 10^{-3} \text{ min}^{-1}$   
254 and  $6.1 \times 10^{-4} \text{ min}^{-1}$ , respectively. Uncertainties on  $J_{calc,VOC}$  were estimated to 20-30%

255 using the error propagation method from the uncertainties on  $\sigma_{\text{VOC}}(\lambda)$  (as reported in  
256 the literature) and  $J_{\text{NO}_2}$  (used to calculate  $F(\lambda)$ ). Effective quantum yields, defined as  
257  $\Phi_{\text{eff}} = J_{\text{VOC,corr}}/J_{\text{calc,VOC}}$  were then derived: 0.23, 0.23, 0.28 and 0.46 for 4H4M2P,  
258 PTD, 3H3M2B and 4H3H, respectively, with combined uncertainties of about 50%.  
259 The PTD effective quantum yield is in excellent agreement with Bouzidi et al. who  
260 obtained 0.20 (Bouzidi et al., 2014a). In the case of 4H4M2P, the obtained quantum  
261 yield compares fairly well with literature: Magneron et al. and Aslan et al. found <  
262 0.20 (Magneron et al., 2003) and 0.15 (Aslan et al., 2017c). For 3H3M2B and 4H3H,  
263 literature data report much lower quantum yields of 0.10 (Aslan et al., 2017b; Bouzidi  
264 et al., 2014b). These discrepancies may be due to i) more uncertainties in the  
265 absorption cross section data in the atmospheric window UV range (4H3H especially)  
266 and ii) lack of data for  $\lambda > 350$  nm while the 3H3M2B and 4H3H are probably still  
267 absorbing (see UV spectra in (Aslan et al., 2017b; Messaadia et al., 2012)).  
268

## 269 **3.2 Photolysis products**

### 270 *3.2.1 Hydroxyketones*

271 Many different oxygenated products have been detected and are reported in Table  
272 S1 to Table S6. The concentrations of the main products were quantified by FTIR or  
273 PTR-MS and corrected for dilution using SF<sub>6</sub> measurements. Note that no other  
274 corrections like carbonyl photolysis or secondary production were applied to product  
275 concentrations. Product molar yields (Y) were calculated by ratioing the corrected  
276 product concentrations ( $\Delta[\text{product}]$ ) to the amount of hydroxyketone consumed  
277 ( $\Delta[\text{hydroxyketone}]$ ):  
278

$$279 \quad Y = \Delta[\text{product}]/\Delta[\text{hydroxyketone}] \quad (\text{Eq.} \\ 280 \quad 3)$$

281  
282 The amount of hydroxyketone reacted was determined from FTIR measurements and  
283 corrected for dilution and wall losses. In the case of experiment 7 (4H3H photolysis  
284 without OH scavenger), a degradation of 4H3H occurred at the injection and the FTIR  
285 data were polluted without possibility to extract a decay rate. Therefore, PTR-MS and  
286 GC-MS data were used to determine  $\Delta[4\text{H3H}]$ . The results are detailed in the next  
287 paragraphs successively for 4H4M2P, 3H3M2B and 4H3H. Reported uncertainties  
288 represent only  $1\sigma$  from the linear fits. Global uncertainties on Y are estimated to be of  
289 the order of 60%, including reactant and product calibration errors (20%) and  
290 uncertainties on wall and dilution loss rate constants (40%). In the case of experiment  
291 7, higher global uncertainties on Y (about a factor of 2) are expected due to larger  
292 errors on  $\Delta[4\text{H3H}]$  (see Figure S1d).  
293

### 294 **4-Hydroxy-4-Methyl-2-Pentanone**

295 Formaldehyde, acetone and formic acid were observed by FTIR spectroscopy as the  
296 main products both in the experiment with OH scavenger (experiment 2) and in that  
297 without OH scavenger (experiment 1). Additional formation of acetic acid and  
298 hydroxyacetone was suggested by PTR-MS. Formation of glyoxal and methylglyoxal  
299 was observed by GC-MS. About 50 ppb of O<sub>3</sub> was observed at the end of the  
300 experiments. All identified products are reported in Tables S1 and S2. Based on the  
301 present work and literature data a simplified mechanism can be drawn for the  
302 atmospheric photolysis 4H4M2P (scheme 1).  
303

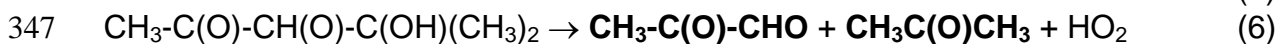
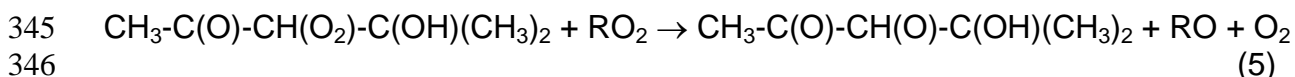




340

341 The hydroxycarbonyl peroxy radical from reaction (1) can also react with another  
342 peroxy radical  $\text{RO}_2$  yielding an alkoxy radical that will decompose into methylglyoxal  
343 and acetone:

344



348

349 The above-suggested mechanism leads to methylglyoxal and acetone formation, as  
350 observed. The enhanced formation of hydroxyacetone in the absence of OH-  
351 scavenger may come from the OH + acetone reaction (Burkholder et al., 2015).

352

353 In their 4H4M2P photolysis experiments using artificial UV-B lamps (275-330 nm, no  
354 OH scavenger), Aslan et al. reported acetone, formaldehyde, and methanol formation  
355 with yields of 1.21, 0.20 and 0.03, respectively (Aslan et al., 2017c). Both the acetone  
356 and formaldehyde yields determined in the present work in the presence of an OH  
357 scavenger are higher than those reported in the literature work. These differences  
358 may be assigned mainly to the different irradiation spectrum used (sunlight vs  
359 artificial) and to uncertainties on  $\Delta$ [hydroxyketone] in the present work. A few ppb of  
360 methanol were observed by FTIR in experiments 1 and 2 and confirmed by PTRMS,  
361 fully consistent with the yield observed by Aslan et al.

362 The acetone yield higher than 1 was attributed to the occurrence of a Norrish II  
363 process implying 4H4M2P intramolecular rearrangement with H-atom transfer (Aslan  
364 et al., 2017c). The present results thus confirm the occurrence of such a process  
365 under sunlight and that photolysis of 4H4M2P is a source of acetone and  
366 formaldehyde in the atmosphere.

367

### 368 **3-Hydroxy-3-Methyl-2-Butanone**

369 For 3H3M2B, acetone, acetic acid and formaldehyde were observed as the main  
370 products by FTIR spectroscopy both in the experiment with and without OH  
371 scavenger (experiments 6 and 5, respectively). PTR-MS measurements confirmed  
372 their formation and showed also acetaldehyde production. The formation of about 30  
373 ppb of  $\text{O}_3$  was observed. All identified products are reported in Tables S3 and S4.

374 Acetone, formaldehyde and acetic acid were quantified by FTIR while acetaldehyde  
375 was quantified by PTR-MS. The corresponding yield plots are displayed on Figures 3  
376 (presence of OH scavenger) and S3 (absence of OH scavenger) while the values are  
377 reported in Table 3. Lower yields were obtained in the absence of OH scavenger  
378 (except for formaldehyde) indicating that the OH + 3H3M2B reaction leads to  
379 different products. Taking into account formaldehyde, acetone, acetaldehyde and  
380 acetic acid, a carbon balance of about nearly 100% is calculated for the experiment  
381 with OH scavenger, whereas a carbon balance of about 75% is calculated for the  
382 experiment without OH scavenger, consistent with the lower product yields obtained.

383

384 In their UV-B photolysis experiments of 3H3M2B, Bouzidi et al. also observed  
385 formaldehyde, acetone and acetic acid as the main products, together with methanol  
386 and CO (Bouzidi et al., 2014b). In the presence of OH scavenger, the reported molar  
387 yields for formaldehyde and acetone were 0.23 and 0.98, in good agreement with the  
388 present results, while a lower formaldehyde yield of 0.16 and a higher acetone yield



422 The reaction of CH<sub>3</sub>-C(O)O<sub>2</sub> with peroxy radicals RO<sub>2</sub> may also lead to acetic acid  
423 (Orlando and Tyndall, 2012):

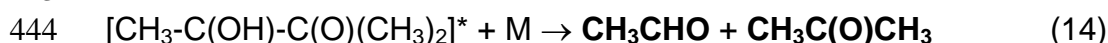
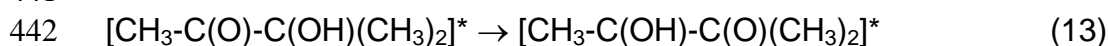
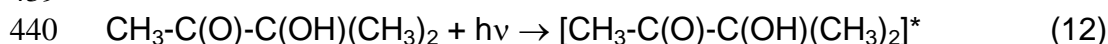


426 R<sub>-H</sub>O represents the carbonyl or alcoholic compound issuing from RO<sub>2</sub>. The yields for  
427 reaction (10) are not known but may partly explain the relatively high acetic acid  
428 yields measured in the present work. Other acetic acid sources from OH reactions  
429 with 3H3M2B or acetaldehyde cannot be excluded.

431 The other photolysis fragment from reaction (7) (C(OH)(CH<sub>3</sub>)<sub>2</sub>) produces acetone and  
432 HO<sub>2</sub> radical by reacting with O<sub>2</sub>:

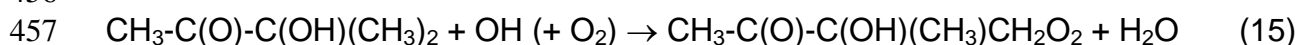


436 Acetaldehyde may be formed through intramolecular rearrangement of an excited  
437 3H3M2B molecule followed by decomposition:

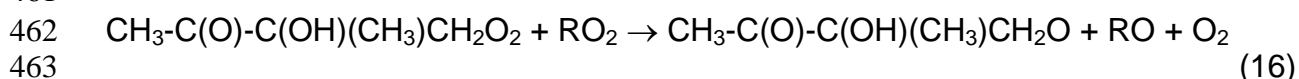


445 M represents N<sub>2</sub> or O<sub>2</sub>. To our knowledge, it is the first time that an intramolecular  
446 rearrangement is proposed for an α-hydroxycarbonyl VOC. The obtained CH<sub>3</sub>CHO  
447 yield of 0.46±0.03 suggests that this last mechanism may represent about 40-50% of  
448 the photolysis of 3H3M2B while the C2 – C3 splitting (leading to acetone and acetic  
449 acid) will last 50-60%. They together lead to an acetone yield of one, fully consistent  
450 with the present experimental findings. This reaction mechanism is different from  
451 Bouzidi et al. who proposed 3H3M2B photolysis through C1 – C2 splitting since  
452 acetic acid was observed as secondary product (Bouzidi et al., 2014b).

453 The lower acetone, acetic acid and acetaldehyde yields determined when the OH  
454 scavenger was absent suggests the following OH-initiated oxidation of 3H3M2B:



458 The radical formed will react with another peroxy radical RO<sub>2</sub> yielding an alkoxy  
459 radical that will decompose into formaldehyde and 2,3-butanedione:

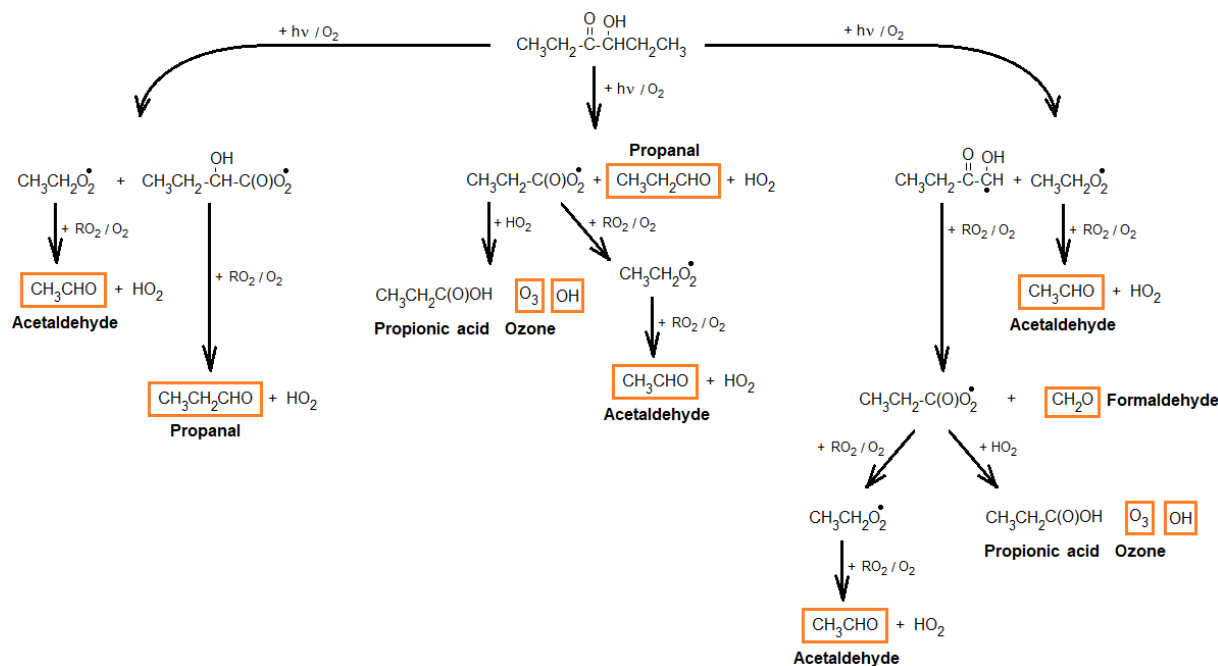


468 LC-MS analysis showed higher amounts of 2,3-butanedione when OH scavenger  
469 was absent, in agreement with this mechanism.

471

472 **4-Hydroxy-3-Hexanone**

473 Acetaldehyde, propanal, acetic acid and formaldehyde were observed as major  
 474 carbonaceous products both in the experiment with and without OH scavenger  
 475 (experiments 8 and 7, respectively). Acetaldehyde and propanal were quantified by  
 476 PTR-MS while formaldehyde and acetic acid were quantified by FTIR. LC-MS  
 477 analysis confirmed the formation of formaldehyde, acetaldehyde and propanal. About  
 478 15 ppb ozone was observed at the end of both experiments. All identified products  
 479 are reported in Tables S5 and S6. Based on the present work, a simplified  
 480 mechanism can be drawn for the atmospheric photolysis of 4H3H (scheme 3).  
 481

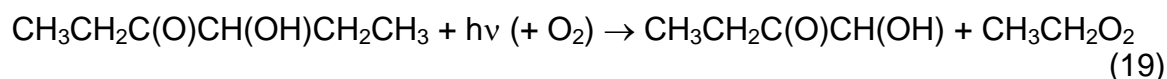


482  
 483  
 484 *Scheme 3: simplified mechanism for 4H3H photolysis; the presence of the species*  
 485 *with orange frame has been confirmed in the present work*  
 486

487 As for the other hydroxyketones, yield plots were constructed for the major products  
 488 (Figures 4 and S4 for experiments with and without OH scavenger, respectively) and  
 489 the yield values are reported in Table 3. Slightly lower yields were obtained in the  
 490 absence of OH-scavenger.

491 The present work representing the first data on 4H3H photolysis products, to our  
 492 knowledge, we propose the following detailed reaction mechanism to explain their  
 493 formation:

- 494  
 495 • After **C4-C5** bond breaking, formaldehyde and acetaldehyde may arise from  
 496 the two radicals generated (reaction (19)):



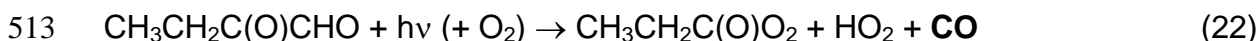
501 The hydroxy-oxy radical  $\text{CH}_3\text{CH}_2\text{C}(\text{O})\text{CH}(\text{OH})$  can either decompose into  
 502 formaldehyde and propionyl radical, the later oxidizing into a propionyl peroxy radical:



505  
506 or form ethylglyoxal by reaction with O<sub>2</sub>:

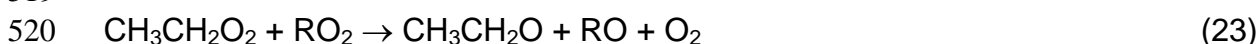


510 Like other  $\alpha$ -dicarbonyls ((Bouzidi et al., 2014a; Szabo et al., 2011)), ethylglyoxal  
511 may be readily photolyzed under sunlight into propionyl peroxy radical, CO and HO<sub>2</sub>:

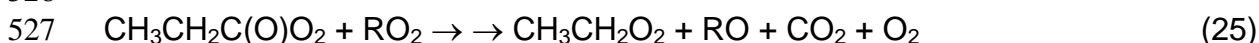


515 Yet, since no CO formation was observed, it is expected that reaction (20) is  
516 preferred to reaction (21).

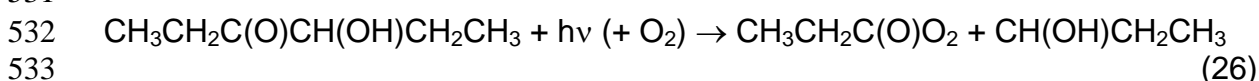
517  
518 The CH<sub>3</sub>CH<sub>2</sub>O<sub>2</sub> radical from reaction (19) will form acetaldehyde through:



523 where RO<sub>2</sub> and RO are peroxy and alkoxy radicals. The CH<sub>3</sub>CH<sub>2</sub>C(O)O<sub>2</sub> formed in  
524 reaction (20) will lead to CH<sub>3</sub>CH<sub>2</sub>O<sub>2</sub> and finally acetaldehyde by reactions with RO<sub>2</sub>  
525 (reactions (25), (23) and (24)):



529 • Acetaldehyde may also come, together with propanal from the **C3-C4** bond  
530 rupture:

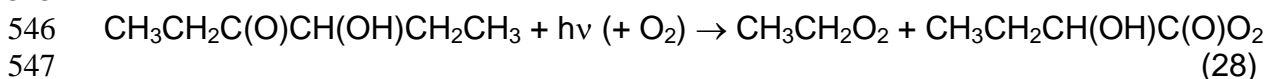


535 followed by



539 As mentioned above, the CH<sub>3</sub>CH<sub>2</sub>C(O)O<sub>2</sub> radical will lead to acetaldehyde (reactions  
540 (23-25)).

541  
542  
543 • Finally, **C2-C3** bond decomposition may also produce acetaldehyde and  
544 propanal via the following reaction sequence:



549 and CH<sub>3</sub>CH<sub>2</sub>O<sub>2</sub> gives CH<sub>3</sub>CHO through (23) and (24). The hydroxyl acylperoxy  
550 radical from reaction (28) reacts with RO<sub>2</sub> to form propanal:



554 The observation of HCHO indicates that the C4-C5 bond breaking channel (the only  
555 one producing HCHO as primary product) is occurring for at least ~36%. In addition,  
556 the observed acetaldehyde yield of about 2 suggests that this last channel is a major  
557 one in the photolysis of 4H3H, since up to two acetaldehyde molecules can be  
558 expected from the photolysis of one 4H3H molecule through the C4-C5 channel. The  
559 two other channels (C3-C4 and C2-C3 bond scissions) specifically form propanal,  
560 indicating their occurrence (at least one of them) in the photolysis of 4H3H. The origin  
561 of acetic acid is not clear: organic acids are generally formed after reactions of  
562 acylperoxy radicals with HO<sub>2</sub>. The above mechanism suggests that only propionyl  
563 peroxy radical (CH<sub>3</sub>CH<sub>2</sub>C(O)O<sub>2</sub>) is formed, enabling propanoic acid to be potentially  
564 formed. Taking into account the observed yields for the four main products, carbon  
565 balances of about 100% for experiments 7 and 8 are obtained.

### 566 3.2.2 2,3-Pentanedione (PTD)

567 As described in the photolysis frequencies part, PTD decomposes much more readily  
568 under sunlight than hydroxyketones. Consequently, the reaction products were  
569 observed in higher amounts and could be quantified more accurately by both FTIR  
570 and PTR-MS.

571 They consisted mainly in formaldehyde, acetaldehyde, acetic and propionic acids,  
572 methanol and ozone. Figure 5 presents the time profiles of PTD and of the main  
573 reaction products as determined from FTIR measurements (except propionic acid  
574 from PTR-MS and ozone from O<sub>3</sub> analyser) for the experiment carried out with OH  
575 scavenger. A similar figure is drawn for the experiment carried out without OH  
576 scavenger (Figure S5). Product yield curves were then plotted (Figures 6 and 7 for  
577 PTR-MS and FTIR data, respectively) and the results are reported in Table 4.  
578 Uncertainties come from IR absorption cross sections (3.3%, 13%, 3.6%, 20% and  
579 10% for formaldehyde, acetaldehyde, acetic acid, methanol and ozone, respectively)  
580 and PTR-MS calibration (30% for all products). Thus, global uncertainties range from  
581 4% (formaldehyde) to 21% (methanol) for FTIR results and are about 30% for PTR-  
582 MS results. The product yield curves obtained from the experiment without OH  
583 scavenger are available in Figures S6 and S7, while the corresponding yields are  
584 gathered in Table 4.

585 Very good agreement was obtained for the product yields from FTIR and PTR-MS  
586 data when both data were available (formaldehyde, acetaldehyde, acetic acid and  
587 methanol). Molar yields obtained by Bouzidi et al. for formaldehyde and acetaldehyde  
588 are also reported in Table 4 and display lower values by ~20% (Bouzidi et al.,  
589 2014a). The present results show satisfactory agreement taking into account the  
590 global uncertainties in both studies.

591 The next step consisted in the numerical simulation of the reactant and product time  
592 profiles based on recommended/known rate constants of the molecular/radical  
593 species implied in the chemical mechanism. The mechanism proposed by Bouzidi et  
594 al. (Bouzidi et al., 2014a) was complemented with the EUPHORE auxiliary  
595 mechanism

596 (<https://www.eurochamp.org/Facilities/SimulationChambers/EUPHORE.aspx>) (Table  
597 S4). Since cyclohexane was introduced as OH-radical scavenger in experiment 4, its  
598 oxidation by OH was included in the mechanism. About 0.1 ppb NO (from  
599 background air) was also added initially as measured by the NO<sub>x</sub> analyser. The PTD  
600 photolysis frequency was adjusted to its measured value and assumed to be  
601 constant over the experiment. The photolysis frequency of CH<sub>2</sub>O was adjusted  
602 towards CO formation rate taking into account a CO detection limit of 18 ppb. FTIR  
603

604 data were used for all compounds except propanoic acid for which only PTR-MS data  
 605 were available. Experiment 3 performed without OH-scavenger was not simulated,  
 606 since the OH + PTD chemical mechanism is largely unknown.

607 The simulated time profiles can be seen on Figure 5 (full lines) for the experiment  
 608 with OH-scavenger. The agreement is very satisfying for formaldehyde,  
 609 acetaldehyde, methanol and ozone. Ozone being produced only from  $\text{CH}_3\text{C}(\text{O})\text{O}_2 +$   
 610  $\text{HO}_2$  (reaction (13c)) and  $\text{C}_2\text{H}_5\text{C}(\text{O})\text{O}_2 + \text{HO}_2$  (reaction (14c)), the agreement  
 611 suggests that the corresponding rate constants and branching ratios are correct. For  
 612 acetic acid, the modelled formation rate appears faster at the beginning, leading to  
 613 about +30% higher concentrations after 1h photolysis; then the differences between  
 614 modelled and experimental concentrations gradually diminish to reach less than 10%.  
 615 Conversely, in the case of propionic acid, experimental concentrations are  
 616 underestimated by up to 30%. Since propionic acid was measured by PTR-MS at  
 617 mass  $M+1 = 75$ , mass interferences from compounds like hydroxyacetone and  
 618 hydroxypropanal cannot be excluded. However, it is difficult to find reactions that can  
 619 yield such compounds in the photolysis of 2,3-pentanedione. Regarding the reaction  
 620 mechanism, two types of reactions leading to propionic acid have to be considered:

621 1)  $\text{C}_2\text{H}_5\text{C}(\text{O})\text{O}_2 + \text{HO}_2$  (reaction (14c)); this reaction also produces  $\text{O}_3$  (together with  
 622 reaction (13c)); since  $\text{O}_3$  is well simulated, this indicates that the branching ratio of  
 623 0.25 (Hasson et al., 2012) leading to propionic acid and  $\text{O}_3$  is probably correct;

624 2)  $\text{C}_2\text{H}_5\text{C}(\text{O})\text{O}_2 + \text{RO}_2$  (reaction (8) for  $\text{RO}_2 = \text{CH}_3\text{O}_2$ , reaction (10) for  $\text{RO}_2 = \text{C}_2\text{H}_5\text{O}_2$   
 625 and reaction (21) for  $\text{RO}_2 = \text{C}_6\text{H}_{11}\text{O}_2$ ). Reaction (10) was studied by (Le Crâne et al.,  
 626 2005) who reported a branching ratio of 0.18 towards  $\text{C}_2\text{H}_5\text{C}(\text{O})\text{OH} + \text{O}_3$ . Reactions  
 627 (8) and (21) were supposed to behave as reaction (8). Therefore, sensitivity tests  
 628 were performed on the channels leading to propionic acid, showing that increasing  
 629 the molecular channel in  $\text{C}_2\text{H}_5\text{C}(\text{O})\text{O}_2 + \text{RO}_2$  from 0.18 to 0.26 allows good  
 630 agreement between experimental and simulated propionic acid concentrations to be  
 631 obtained (Figure 5: full lines are with 0.18 while dashed lines are with 0.26). The  
 632 present results indicate that more work is needed on  $\text{RC}(\text{O})\text{O}_2 + \text{RO}_2$  cross reactions  
 633 to clarify kinetics and mechanisms.

634

### 635 3.3 Structure activity relationships

636 Considering the  $J_{\text{VOC,corr}}/J_{\text{NO}_2}$  ratios in Table 2 shows that 2,3-pentanedione is much  
 637 more photolabile than  $\alpha$ - and  $\beta$ -hydroxyketones. This is probably due to the  
 638 conjugated inductive effect of the two  $-\text{C}(\text{O})$  functions in PTD in lowering the C2-C3  
 639 bond energy. Such high photolytic activity is also observed for glyoxal and  
 640 methylglyoxal (Moortgat, 2001).

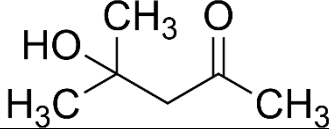
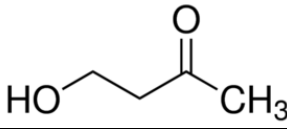
641 In terms of hydroxyketone reactivity, comparing 3H3M2B ( $J_{\text{VOC,corr}}/J_{\text{NO}_2} = 8.2 \times 10^{-4}$ )  
 642 and 4H3H ( $J_{\text{VOC,corr}}/J_{\text{NO}_2} = 5.1 \times 10^{-4}$ ), methyl substitution on the carbon atom bearing  
 643 the OH group seems to increase photolysis ability.

644

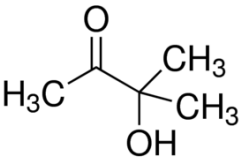
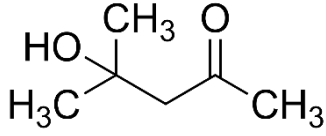
Compound	3-hydroxy-3-methyl-2-butanone	4-hydroxy-3-hexanone
$J_{\text{VOC,corr}}/J_{\text{NO}_2}$	$8.2 \times 10^{-4}$	$5.1 \times 10^{-4}$

645

646 This is confirmed when comparing 4H4M2P ( $J_{VOC,corr}/J_{NO_2} = 6.2 \times 10^{-4}$ ) to 4-hydroxy-2-  
 647 butanone ( $CH_3-C(O)-CH_2-CH_2OH$ ), where a  $J_{VOC}/J_{NO_2}$  of  $1.8 \times 10^{-5}$  can be calculated  
 648 from (Bouzidi et al., 2015a).  
 649

Compound	4-hydroxy-4-methyl-2-pentanone	4-hydroxy-2-butanone
		
$J_{VOC,corr}/J_{NO_2}$	$6.2 \times 10^{-4}$	$1.8 \times 10^{-5}$

650  
 651 Increasing the distance between the carbonyl and hydroxyl groups lowers photolysis  
 652 reactivity, as in 4H4M2P ( $J_{VOC,corr}/J_{NO_2} = 6.2 \times 10^{-4}$ ) compared to 3H3M2B  
 653 ( $J_{VOC,corr}/J_{NO_2} = 8.2 \times 10^{-4}$ ).  
 654

Compound	3-hydroxy-3-methyl-2-butanone	4-hydroxy-4-methyl-2-pentanone
		
$J_{VOC,corr}/J_{NO_2}$	$8.2 \times 10^{-4}$	$6.2 \times 10^{-4}$

655  
 656 Regarding reaction mechanisms, because of the relatively high uncertainties on  
 657 product yields, it is difficult to give general trends. Yet, the present work showed that  
 658 photolysis of hydroxyketones proceeds through different initial C-C bond scissions  
 659 (Norrish I type) and that some of them undergo intramolecular rearrangement  
 660 (Norrish II type). In addition, it has been demonstrated that sunlight photolysis of the  
 661 investigated hydroxyketones gives rise to carbonyl species of atmospheric interest  
 662 like acetone and formaldehyde.  
 663

#### 664 4. Atmospheric implications

665 The photolysis frequencies summarized in Table 2 can be used to estimate the half  
 666 lifetime ( $\tau_{1/2}$ ) of the investigated carbonyls towards photolysis. This half lifetime can  
 667 be retrieved according to:

$$669 \tau_{1/2} = \frac{\ln 2}{J_{VOC,corr}} \quad (\text{Eq. } 4)$$

670  
 671  
 672 A half lifetime of about 40 min is obtained for PTD, while much larger  $\tau_{1/2}$  values of  
 673 about 1-2 days are calculated for hydroxyketones. PTD has a half lifetime of about 4  
 674 days towards OH radicals, assuming an average OH concentration of  $1 \times 10^6$  radicals  
 675  $cm^{-3}$  (Szabo et al., 2011). The present results allow confirming that photolysis is by  
 676 far the main oxidation pathway of PTD in the atmosphere, as for other  $\alpha$ -dicarbonyls  
 677 (Moortgat, 2001). Rate constants of hydroxyketones with OH (in  $cm^3 \text{ molecule}^{-1} \text{ s}^{-1}$ )  
 678 are  $4.3 \times 10^{-12}$ ,  $7.6 \times 10^{-13}$  and  $1.5 \times 10^{-11}$  at 298 K for 4H4M2P (Aslan et al., 2017c),  
 679 3H3M2B (Bouzidi et al., 2014b) and 4H3H (Aschmann et al., 2000), respectively,  
 680 leading to half lifetimes of 2 days, 10 days and 0.5 day (Table 2). Thus, photolysis  
 681 appears to be a competitive degradation process for 4H4M2P and 3H3M2B while it is  
 682 less important for 4H3H. Note that the acetone photolysis lifetime calculated at 55°N  
 683 is about 100 days (Singh et al., 1994), suggesting a significant effect of the hydroxyl

684 group on the photolysis reactivity of hydroxyketones. The present work underlines the  
685 need to take into account the photolysis of multifunctional carbonyls as a direct  
686 radical and carbonyl source in the atmosphere.

#### 687 **Data availability.**

689 Experimental data will be available in the Eurochamp database,  
690 [www.eurochamp.org](http://www.eurochamp.org), from the H2020 EUROCHAMP2020 project, GA no. 730997

691

#### 692 **Acknowledgements**

693

694 The authors gratefully thank the INSU-LEFE French program for financial support.  
695 SAGE and PC2A laboratory participates in the Labex CaPPA (Chemical and Physical  
696 Properties of the Atmosphere, ANR-11-Labx-0005-01) supported by the French  
697 research agency ANR, and in the Climibio program supported by the Hauts-de-  
698 France Regional Council, the French Ministry of Higher Education and Research and  
699 the European Regional Development Fund. L. Aslan is grateful for a PhD scholarship  
700 from the Hauts-de-France Regional Council and IMT Lille Douai. This work has  
701 received funding from the European Union's Horizon 2020 research and innovation  
702 programme through the EUROCHAMP-2020 Infrastructure Activity under grant  
703 agreement No. 730997, by means of its Transnational Activities, and the IMAGINA-  
704 Prometeo project PROMETEO 2019/110). Fundación CEAM is partly supported by  
705 Generalitat Valenciana.

706

#### 707 **References**

708

709 Aschmann, S. M., Arey, J., and Atkinson, R.: Atmospheric chemistry of selected  
710 hydroxycarbonyls, *J. Phys. Chem. A*, 104, 3998–4003, 2000.

711 Aslan, L., Priya, A. M., Sleiman, C., Zeineddine, M. N., Coddeville, P., Fittschen, C.,  
712 Ballesteros, B., Canosa, A., Senthilkumar, L., El Dib, G., and Tomas, A.: Experimental and  
713 theoretical investigations of the kinetics and mechanism of the Cl + 4-hydroxy-4-methyl-2-  
714 pentanone reaction, *Atmos. Environ.*, 166, 315–326, 2017a.

715 Aslan, L., Laversin, H., Roth, E., Coddeville, P., Fittschen, C., Chakir, A., and Tomas, A.:  
716 Gas-phase UV absorption cross-sections and photolysis kinetics of 4-hydroxy-3-hexanone:  
717 Atmospheric implications, *Chem. Phys. Lett.*, 688, 43–46, 2017b.

718 Aslan, L., Laversin, H., Coddeville, P., Fittschen, C., Roth, E., Tomas, A., and Chakir, A.:  
719 Kinetics of the photolysis and OH reaction of 4-hydroxy-4-methyl-2-pentanone: Atmospheric  
720 implications, *Atmos. Environ.*, 150, 256–263, 2017c.

721 Aumont, B., Szopa, S., and Madronich, S.: Modelling the evolution of organic carbon during  
722 its gas-phase tropospheric oxidation: development of an explicit model based on a self  
723 generating approach, *Atmospheric Chem. Phys.*, 5, 2497–2517, 2005.

724 Becker, K. H.: The European Photoreactor EUPHORE, BUGH Wuppertal (Germany),  
725 Wuppertal, 1996.

726 Borrás, E., Ródenas, M., Vera, T., Gómez, T., and Muñoz, A.: Atmospheric degradation of  
727 the organothiophosphate insecticide – Pirimiphos-methyl, *Sci. Total Environ.*, 579, 1–9,  
728 <https://doi.org/10.1016/j.scitotenv.2016.11.009>, 2017.

- 729 Bouzidi, H., Fittschen, C., Coddeville, P., and Tomas, A.: Photolysis of 2,3-pentanedione and  
730 2,3-hexanedione: kinetics, quantum yields, and product study in a simulation chamber,  
731 *Atmos. Environ.*, 82, 250–257, 2014a.
- 732 Bouzidi, H., Laversin, H., Tomas, A., Coddeville, P., Fittschen, C., El Dib, G., Roth, E., and  
733 Chakir, A.: Reactivity of 3-hydroxy-3-methyl-2-butanone: Photolysis and OH reaction  
734 kinetics, *Atmos. Environ.*, 98, 540–548, 2014b.
- 735 Bouzidi, H., Aslan, L., El Dib, G., Coddeville, P., Fittschen, C., and Tomas, A.: Investigation  
736 of the gas-phase photolysis and temperature-dependent OH reaction kinetics of 4- hydroxy-2-  
737 butanone, *Environ. Sci. Technol.*, 49, 12178–12186, 2015a.
- 738 Bouzidi, H., Djehiche, M., Gierczak, T., Morajkar, P., Fittschen, C., Coddeville, P., and  
739 Tomas, A.: Low pressure photolysis of 2,3-pentanedione in air: quantum yields and reaction  
740 mechanism, *J. Phys. Chem. A*, 119, 12781–12789, 2015b.
- 741 Bouzidi, H., Djehiche, M., Coddeville, P., Fittschen, C., and Tomas, A.: Atmospheric  
742 chemistry of  $\alpha$ -diketones: Kinetics of C5 and C6 compounds with Cl atoms and OH radicals,  
743 *Int. J. Chem. Kinet.*, 49, 112–118, 2017.
- 744 Burkholder, J. B., Sander, S. P., Abbatt, J. P. D., Barker, J. R., Huie, R. E., Kolb, C. E.,  
745 Kurylo, M. J., Orkin, V. L., Wilmouth, D. M., and Wine, P. H.: *Chemical Kinetics and  
746 Photochemical Data for Use in Atmospheric Studies, Evaluation No. 18, Jet Propulsion  
747 Laboratory, Pasadena, 2015.*
- 748 Calvert, J. G., Mellouki, A., Orlando, J. J., Pilling, M. J., and Wallington, T. J.: *The  
749 mechanisms of atmospheric oxidation of the oxygenates, Oxford University Press, New York,  
750 2011.*
- 751 Demerjian, K. L., Schere, K. L., and Peterson, J. T.: Theoretical estimates of actinic  
752 (spherically integrated) flux and photolytic rate constants of atmospheric species in the lower  
753 troposphere, *Adv. Environ. Sci. Technol.*, 10, 369–459, 1980.
- 754 Grosjean, E. and Grosjean, D.: The gas-phase reaction of alkenes with ozone: formation  
755 yields of carbonyls from biradicals in ozone-alkene-cyclohexane experiments, *Atmos.  
756 Environ.*, 32, 3393–3402, 1998.
- 757 Hasson, A. S., Tyndall, G. S., Orlando, J. J., Singh, S., Hernandez, S. Q., Campbell, S., and  
758 Ibarra, Y.: Branching ratios for the reaction of selected carbonyl-containing peroxy radicals  
759 with hydroperoxy radicals, *J. Phys. Chem. A*, 116, 6264–6281, 2012.
- 760 Hodzic, A., Madronich, S., Kasibhatla, P. S., Tyndall, G., Aumont, B., Jimenez, J. L., Lee-  
761 Taylor, J., and Orlando, J.: Organic photolysis reactions in tropospheric aerosols: effect on  
762 secondary organic aerosol formation and lifetime, *Atmospheric Chem. Phys.*, 15, 9253–9269,  
763 <https://doi.org/10.5194/acp-15-9253-2015>, 2015.
- 764 Le Crâne, J.-P., Villenave, E., Hurley, M. D., Wallington, T. J., and Ball, J. C.: Atmospheric  
765 chemistry of propionaldehyde: Kinetics and mechanisms of reactions with OH radicals and Cl  
766 atoms, UV spectrum, and self-reaction kinetics of CH<sub>3</sub>CH<sub>2</sub>C(O)O<sub>2</sub> radicals at 298 K, *J.  
767 Phys. Chem. A*, 109, 11837–11850, 2005.

- 768 Magneron, I., Bossoutrot, V., Mellouki, A., Laverdet, G., and Le Bras, G.: The OH-initiated  
769 oxidation of hexylene glycol and diacetone alcohol, *Environ. Sci. Technol.*, 37, 4170–4181,  
770 2003.
- 771 Messaadia, L., El Dib, G., Ferhati, A., Roth, E., and Chakir, A.: Gas phase UV absorption  
772 cross-sections for a series of hydroxycarbonyls, *Chem. Phys. Lett.*, 529, 16–22, 2012.
- 773 Messaadia, L., El Dib, G., Ferhati, A., and Chakir, A.: UV–visible spectra and gas-phase rate  
774 coefficients for the reaction of 2,3-pentanedione and 2,4-pentanedione with OH radicals,  
775 *Chem. Phys. Lett.*, 626, 73–79, 2015.
- 776 Moortgat, G. K.: Important photochemical processes in the atmosphere, *Pure Appl. Chem.*,  
777 73, 487–490, 2001.
- 778 Morgan, R. B. and Jackson, A. V.: Measurements of gas-phase hydrogen peroxide and methyl  
779 hydroperoxide in the coastal environment during the PARFORCE project, *J. Geophys. Res.*  
780 *Atmospheres*, 107, <https://doi.org/10.1029/2000JD000257>, 2002.
- 781 Muñoz, A., Vera, T., Sidebottom, H., Mellouki, A., Borrás, E., Ródenas, M., Clemente, E.,  
782 and Vázquez, M.: Studies on the Atmospheric Degradation of Chlorpyrifos-Methyl, *Environ.*  
783 *Sci. Technol.*, 45, 1880–1886, <https://doi.org/10.1021/es103572j>, 2011.
- 784 Muñoz, A., Borrás, E., Ródenas, M., Vera, T., and Pedersen, H. A.: Atmospheric Oxidation of  
785 a Thiocarbamate Herbicide Used in Winter Cereals, *Environ. Sci. Technol.*, 52, 9136–9144,  
786 <https://doi.org/10.1021/acs.est.8b02157>, 2018.
- 787 Orlando, J. J. and Tyndall, G. S.: Laboratory studies of organic peroxy radical chemistry: an  
788 overview with emphasis on recent issues of atmospheric significance, *Chem. Soc. Rev.*, 41,  
789 6294–6317, 2012.
- 790 Reisen, F., Aschmann, S. M., Atkinson, R., and Arey, J.: Hydroxyaldehyde products from  
791 hydroxyl radical reactions of *z*-3-hexen-1-ol and 2-methyl-3-buten-2-ol quantified by SPME  
792 and API-MS, *Environ. Sci. Technol.*, 37, 4664–4671, 2003.
- 793 Singh, H. B., O’Hara, D., Herlth, D., Sachse, W., Blake, D. R., Bradshaw, J. D., Kanakidou,  
794 M., and Crutzen, P. J.: Acetone in the atmosphere: Distribution, sources and sinks, *J.*  
795 *Geophys. Res.*, 99, 1805–1819, 1994.
- 796 Szabo, E., Djehiche, M., Riva, M., Fittschen, C., Coddeville, P., Sarzynski, D., Tomas, A.,  
797 and Dobé, S.: Atmospheric chemistry of 2,3-pentanedione: Photolysis and reaction with OH  
798 radicals, *J. Phys. Chem. A*, 115, 9160–9168, 2011.
- 799 Thalman, R., Baeza-Romero, M. T., Ball, S. M., Borrás, E., Daniels, M. J. S., Goodall, I. C.  
800 A., Henry, S. B., Karl, T., Keutsch, F. N., Kim, S., Mak, J., Monks, P. S., Muñoz, A.,  
801 Orlando, J., Peppe, S., Rickard, A. R., Ródenas, M., Sánchez, P., Seco, R., Su, L., Tyndall,  
802 G., Vázquez, M., Vera, T., Waxman, E., and Volkamer, R.: Instrument intercomparison of  
803 glyoxal, methyl glyoxal and NO<sub>2</sub> under simulated atmospheric conditions, *Atmospheric*  
804 *Meas. Tech.*, 8, 1835–1862, <https://doi.org/10.5194/amt-8-1835-2015>, 2015.
- 805 Tomas, A., Villenave, E., and Lesclaux, R.: Reactions of the HO<sub>2</sub> radical with CH<sub>3</sub>CHO and  
806 CH<sub>3</sub>C(O)O<sub>2</sub> in the gas phase, *J. Phys. Chem. A*, 105, 3505–3514, 2001.

807 Tuazon, E. C., Aschmann, S. M., Arey, J., and Atkinson, R.: Products of the gas-phase  
808 reactions of a series of methyl-substituted ethenes with the OH radical, *Environ. Sci.*  
809 *Technol.*, 32, 2106–2112, 1998.

810 Winiberg, F. A. F., Dillon, T. J., Orr, S. C., Gross, C. B. M., Bejan, I., Brumby, C. A., Evans,  
811 M. J., Smith, S. C., Heard, D. E., and Seakins, P. W.: Direct measurement of OH and other  
812 product yields from the HO<sub>2</sub> + CH<sub>3</sub>C(O)O<sub>2</sub> reaction, *Atmospheric Chem. Phys.*, 16, 4023–  
813 4042, 2016.

814